IDE❖L®

Transient Magnetic Resonance without RF Pulses: Fast Field Switching

David J. Sloop, Tien-Sung Lin, and Joseph J. H. Ackerman[1]

Department of Chemistry, Campus Box 1134, Washington University, One Brookings Drive, St. Louis, Missouri 63130-4899

An unusual strategy for performing magnetic resonance experiments is demonstrated. Instead of employing conventional radiofrequency transmitter fields to perturb spin state populations away from equilibrium, as is the basis of most magnetic resonance spectrometers today, technological advances now make possible fast switching of the magnetic field orientation to achieve the same effect. This is demonstrated with an electron spin resonance experiment where the magnetic field is switched 90° nonadiabatically with a dead time of a few tens of nanoseconds and an electron free induction decay observed.   © 1999 Academic Press

Key Words: **EPR; instrumentation; spectrometer; radiofrequency.**

INTRODUCTION

Magnetic resonance (MR), both nuclear and electron, has become a vitally important tool in research and clinical settings spanning an astonishing range of applications. Indeed, the great commercial and health care related success of magnetic resonance imaging is often cited as the prototypical illustration of the value to society of basic science research such as the early path breaking MR experiments of Rabi, Bloch, and Purcell.

Following half a century of technological evolution, MR instruments today rely nearly exclusively on either exposing a sample to short bursts of high frequency magnetic fields (for perturbation of nuclear or electron spin state populations) while the samples are bathed in relatively large fixed magnetic fields, or, to the same effect, on slowly sweeping large magnetic fields in a continuous manner while the samples are exposed to low-power high-frequency magnetic fields. In either case, a strong, highly homogeneous and stable, static magnetic field is employed to produce the initial population differential among spin states, *i.e.,* to induce magnetic polarization.

An alternative approach does exist, one that in certain instances may offer advantages to the use of RF transmitter fields in MR. Here we refer to fast field switching.

The concept of fast field switching (FFS) magnetic resonance was presaged by Packard and Varian in 1954 in their description of a means to observe free nuclear induction in the earth's magnetic field following the abrupt cessation of a strong polarizing field (*1*). Abragam, in his classic text, described such an approach as an "elegant alternative" to the use of an RF transmitter field (*2a*). Representative additional examples of continued interest in this strategy for nuclear magnetic resonance applications include Earth's field imaging (*3*), spin relaxation (*4*), field cycling (*5–7*), and numerical solution of the Bloch equation (*8*). Herein, high-speed MOSFET derives are used in a non-energy-conserving circuit to obtain $dB/dt > 10^5$ *T*/s over a small sample volume and observe a field switched *electron* paramagnetic resonance (EPR) signal. The spectrometer was constructed to examine the possibility of medical EPR imaging at low fields without using RF pulses.

METHODS

The essence of the experiment, in simplest form, is the following: (i) the sample's electron spins are equilibrated in the polarizing magnetic field for a period on the order of the spin–lattice relaxation time, T_1; (ii) the polarizing field is rapidly reduced to near zero in a time short relative to T_1; (iii) an orthogonal magnetic field is imposed in a time short compared to the transverse or spin–spin relaxation time, T_2, as the polarizing field nears zero, and (iv) the response of the sample magnetization, now precessing about the new magnetic field axis, is monitored via high-speed digitizing hardware.

To demonstrate this principle, an experiment was performed in a 185-MHz (6.6 mT) FFS spectrometer designed and constructed in our laboratory. Figure 1 schematically illustrates the FFS spectrometer, Fig. 2 illustrates the coil geometry, and Fig. 3 describes the field switching timing of the experiment.

Initially, pulses of electric current applied through a pair of 5-mm-diameter Helmholtz coils around the sample produce a polarizing magnetic field, $\mathbf{B}_0$, of 44 mT with duration of several T_1's to achieve significant electron spin polarization. Here we take $\mathbf{B}_0$ to be applied along the *y* axis. The FFS experiment requires that the magnetic field be *nonadiabatically* switched, nominally 90°, from the $\mathbf{B}_0$ axis used to polarize the spins; $dB/dt \geq 4\ \gamma_e\ \mathbf{B}_0^2$ (*8*). $\mathbf{B}_0$ is first reduced to near zero, $\mathbf{B}_0 < 0.4$ mT, to avoid spin locking of the polarization to a *rotating* field. Immediately following this, an orthogonal precessional field, $\mathbf{B}_0^*$, of 6.6 mT is switched on by pulsing an

[1] To whom correspondence should be addressed. Fax: 314-935-4481. E-mail: ackerman@wuchem.wustl.edu.
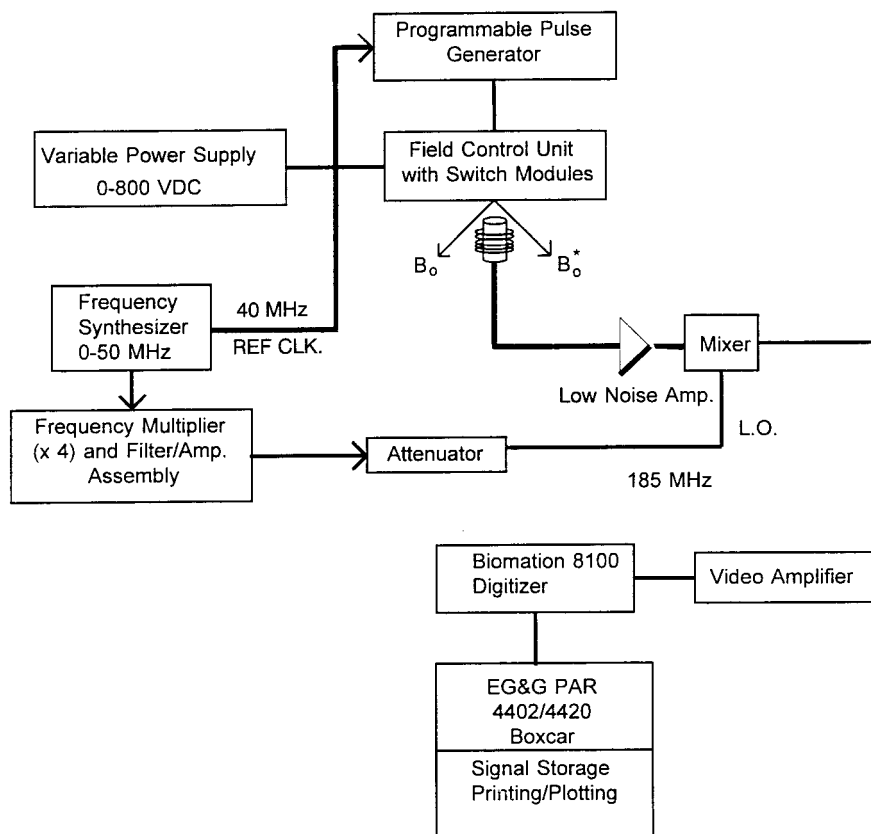
Fast Field Switching Spectrometer
Block Diagram

Programmable Pulse Generator

Variable Power Supply 0-800 VDC

Field Control Unit with Switch Modules

B_o B_o^*

Frequency Synthesizer 0-50 MHz

40 MHz
REF CLK.

Low Noise Amp. **Mixer**

Frequency Multiplier (x 4) and Filter/Amp. Assembly

Attenuator

L.O.

185 MHz

Biomation 8100 Digitizer

Video Amplifier

EG&G PAR 4402/4420 Boxcar

Signal Storage Printing/Plotting

FIG. 1. A block diagram illustrating the 185-MHz fast field switching (FFS) spectrometer. The field switching unit is composed of four high-power MOSFET switching modules connected to individual field switching Helmholtz coil elements mounted around the sample as diagrammed in Fig. 2. The sample has a frequency-tuned and impedance-matched signal pickup coil around it with the coil axis orthogonal to the plane containing the field switching coil axes. The pickup coil is matched to the 50-ohm input impedance of the Miteq preamplifier. The signal is routed to the low noise preamplifier and mixer through semi-rigid 0.141-in.-diameter coaxial cables. The signal from the mixer is further amplified in the video amplifier, stored in a Biomation multichannel analyzer, and downloaded to an EG&G signal averaging boxcar. The operating frequency is derived from a frequency synthesizer and multiplier chain. The local oscillator arm of the high-level mixer operates at 12 dBm. The field current control pulses that drive the field switching units are generated by the field control unit from instructions delivered by the main computer through an IEEE488 interface.

electric current through an orthogonal pair of 13-mm-diameter Helmholtz coils. The magnetic moment due to the sample electron spin paramagnetism then precesses at 185 MHz about the $\mathbf{B}_0^*$ axis. Here we take this to be the x axis. Calculated magnetic field amplitude vs time profiles for the prototype system employed herein are illustrated in Fig. 3.

Figure 4a is a functional diagram showing circuitry for one pair of magnetic field switching coils. Figure 4b is a schematic diagram showing a circuit assembly that includes a magnetic field coil, resistor, capacitor energy storage bank on a circuit board, and MOSFET switch module. The spectrometer described here uses four such assemblies, with the field coils arranged as shown in Fig. 2. The switch modules are driven by synchronized TTL level pulses to control the time-dependent magnetic fields along the y and x coil axes.

The capacitance totals on the energy storage circuit boards are selected to limit the voltage discharge during the polarizing field pulse to less than 5% and the observation field pulses to less than 0.25%. Diode D1 is an ultrafast 600V STTA806D component made by SGS-Thompson Microelectronics connected to limit the voltage across the MOSFET. MOSFET transistors (No. DE275, Direct Energy, Inc. Ft. Collins, CO) were used as the high-speed switching elements. This family of MOSFETs was selected due to their high switching speed, high pulsed drain current, and low insertion inductance (1.5 nH). Capacitors are 1-kV, 0.1-mfd low-inductance disk ceramics in parallel with larger electrolytics for energy storage arranged as 30 × 0.1 mfd soldered across double-sided printed circuit FR-4 board material with 2 oz copper laminate for low impedance.
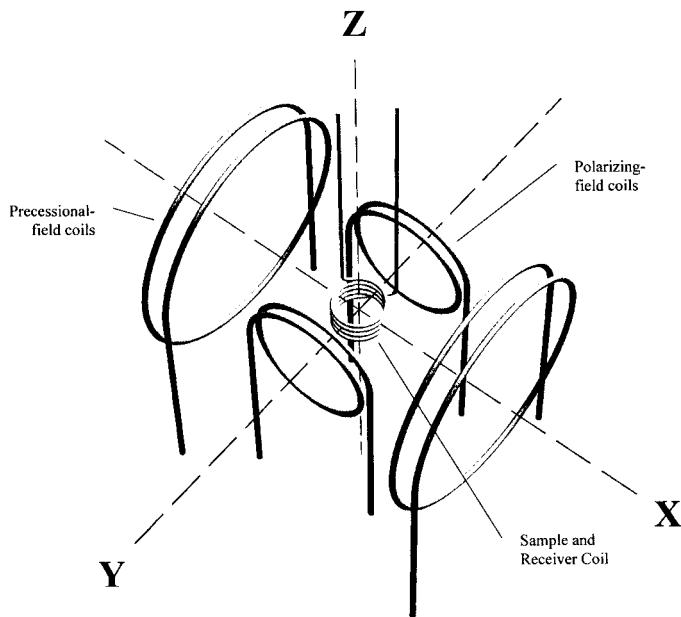
FIG. 2. An illustration showing the geometrical arrangement of the $\mathbf{B}_0$ 5-mm-diameter polarizing-field coils oriented along the y axis, the $\mathbf{B}_0^*$ 13-mm-diameter precessional-field coils oriented along the x axis, and the radiofrequency-receiver coil oriented along the z axis.

Resistors are composed of low-inductance 2-w carbon composition (Allen-Bradley RCR42 HB) elements. A circuit board containing a MOSFET and gate driving circuit (now available from Directed Energy, Inc. Model FPS-3N) that accepts TTL level input is mounted parallel to each energy

storage board that contains the high-voltage and ground plane layers.

Signal detection employs a broadband video amplifier (Model No. 115, Princeton Applied Research, Princeton, NJ) with a bandwidth of 20 MHz and a gain of 60 dB. The receiver preamplifier is broadband (1–500 MHz, Model No. AU-1054, Miteq, Hauppauge, NY) with 2.0 dB noise figure in a homodyne circuit with double-balanced mixer. The receiver coil is wound of No. 40 wire around a 1.5-mm-outer-diameter glass pipette tip used as a sample container. This coil is tuned to parallel resonance at 185 MHz and impedance matched to the Miteq preamplifier 50 ohms input resulting in a coupled resonator loaded Q of approximately 10.

The time required to create a relatively stable magnetic field in an inductive circuit is a function of the ratio of inductance to circuit resistance, L/R. Litz wire elements, with many individually insulated small diameter conductors, are used in the coils to allow the rapidly changing magnetic field to more evenly penetrate the sample volume. The use of Litz wire has the additional experimental convenience that as the sample and pulse coil volumes are increased, the limitations of the MOSFETs and resistors can be balanced against the increased voltage and current requirements summarized in Fig. 5 by simply increasing the number of parallel driven circuit L and R elements. In this experiment, an L/R ratio of the order of 10^{-9} was achieved using modified Litz wire (type 175/40 SPNSN, MWS Wire Industries, Westlake Village, CA), with conductors of No. 40 insulated wire connected in series/parallel with 10-ohm 2-w carbon composition resistors. During the experiments,
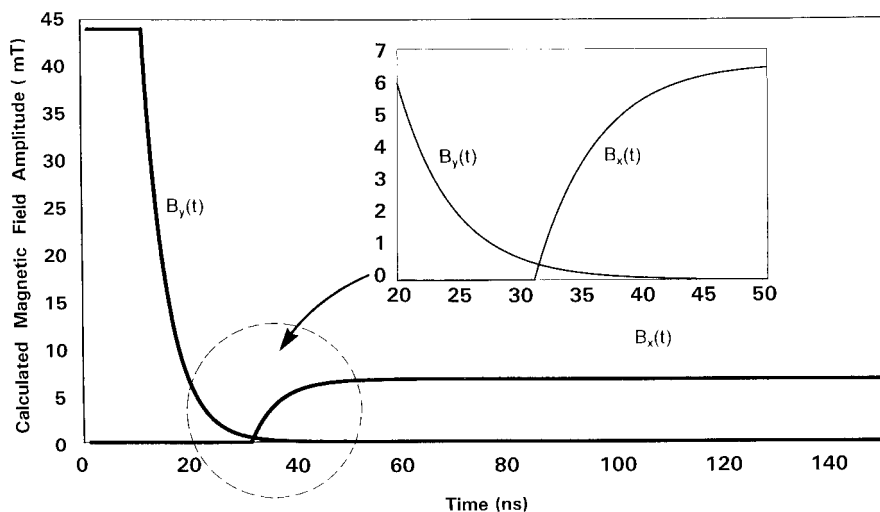

FIG. 3. A depiction of the calculated time-dependent polarizing field, $\mathbf{B}_0 = B_y(t)$ and precessional field, $\mathbf{B}_0^* = B_x(t)$, amplitudes. Insert is an expansion of the 20- to 50-ns region. The polarizing field is turned on well before the $t = 0$ origin used in this illustration and switched off (at $t = 20$ ns in the figure) after significant electron polarization has been achieved, e.g., after ca. 10 μs. A transition time of ca. 20 ns is used to switch from the 44-mT polarizing field along the y axis to the more homogeneous 6.6-mT observation field along the x axis. The polarizing field is brought exponentially to less than 0.4 mT before the observation field is applied. The nonadiabatically applied $B_x(t)$ observation field causes the paramagnetic sample magnetization to precess in the z–y plane.
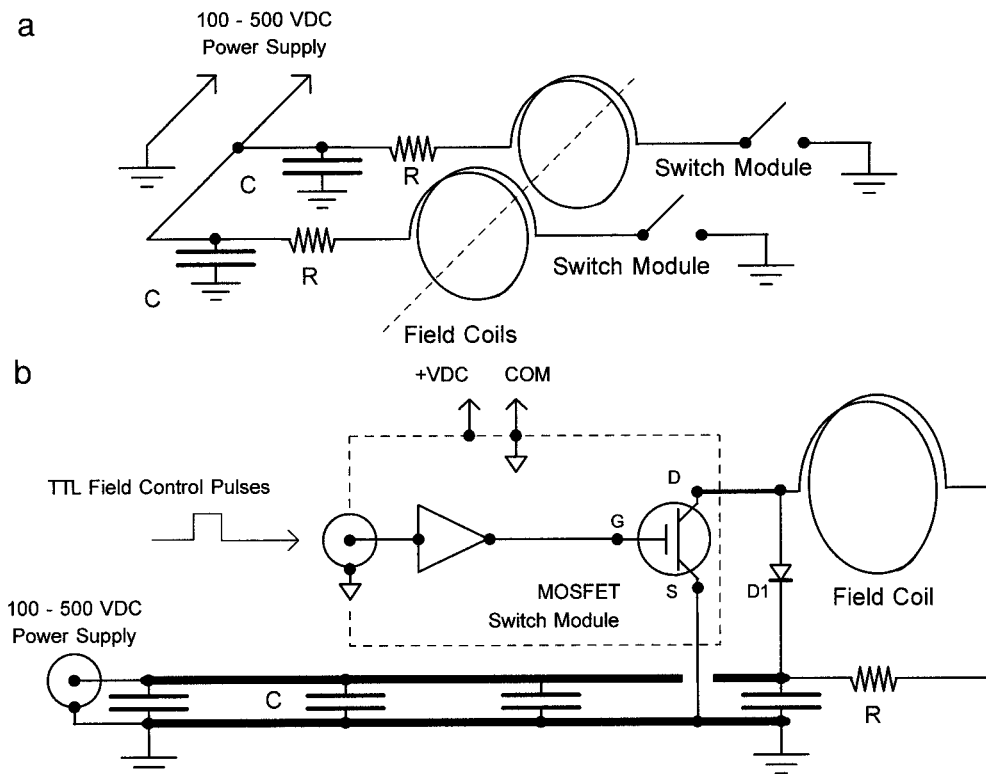
FIG. 4. An illustration depicting the field switching concept (a) and high-speed field switching module and circuit (b). Each switching module has a bank of low-inductance energy storage capacitors soldered across opposite sides of double-sided FR-4 circuit board mounted adjacent to the power MOSFET and gate driving circuit to supply the high currents for the Helmholtz field coils. The MOSFETs (DE-275) and gate driving circuit (FPS-3N) are commercially available from Directed Energy, Inc. The voltage limiting diode D1 is an SGS-Thompson Microelectronics STTA806D.

temperature stability was improved by blowing cool dry nitrogen gas over the resistors and MOSFETs.

THEORY

The modified Bloch equations discussed in Abragam (*2b*) are used to calculate the time dependence of the magnetization, **M**, for simple paramagnetic systems immersed in time-dependent magnetic fields, **B**, such as those shown in Fig. 3.

$$\frac{d\mathbf{M}}{dt} = \gamma \cdot \mathbf{M} \times B(t) - \frac{\mathbf{M} - \chi \cdot \mathbf{B}(t)}{T}. \qquad [1]$$

M is assumed to undergo relaxation toward the instantaneous value of **B**(*t*) with a characteristic relaxation time constant *T*. Figure 6 shows solutions to this equation and the simulated spectrometer response (bold) during the 150-ns magnetic field switching time interval depicted in Fig. 3. The simulated spectrometer response plot assumes a receiver mixer reference frequency of 195 MHz, a display bandwidth of 20 MHz, and a radiofrequency receiver coil tuned to 185 MHz with a loaded Q of 10 and no dead time or induced transient noise.

RESULTS AND DISCUSSION

Approximately 0.13 mm^3 fluoranthenyl radical cation salt of PF$_6$ mounted in a 1.5-mm glass pipette tip was employed as the paramagnetic sample in the initial experiments reported herein. This salt gives a single narrow EPR peak ($\Delta B_{pp} = 5$ μT for $\mathbf{B}_0^*$ parallel to the long needle axis) and the small sample volume fits within the small Helmholtz polarizing and observation field coils. The electron relaxation times were estimated from magnetization saturation experiments carried out on a conventional EPR spectrometer, $T_1 = T_2 = 7$ μs. The FFS FID signal was acquired with a transient waveform recorder (model 8100, Biomation Corp, Cupertino, CA) and further processed in a boxcar signal processor (Model No. 4402/4420 with Model No. 4422 plug-in modules, EG&G PARC, Princeton Applied Research). These instruments were used primarily because of their availability and could now be easily replaced by a high-speed digitizing oscilloscope with sufficient memory. The free-induction decay (FID) obtained by the FFS spectrometer is shown in Fig. 7.

The signal voltage induced in a receiver coil tuned to resonance at the electron spin Larmor frequency will increase at a rate on the order of $Q/\pi f_0$, where Q is the coil quality factor
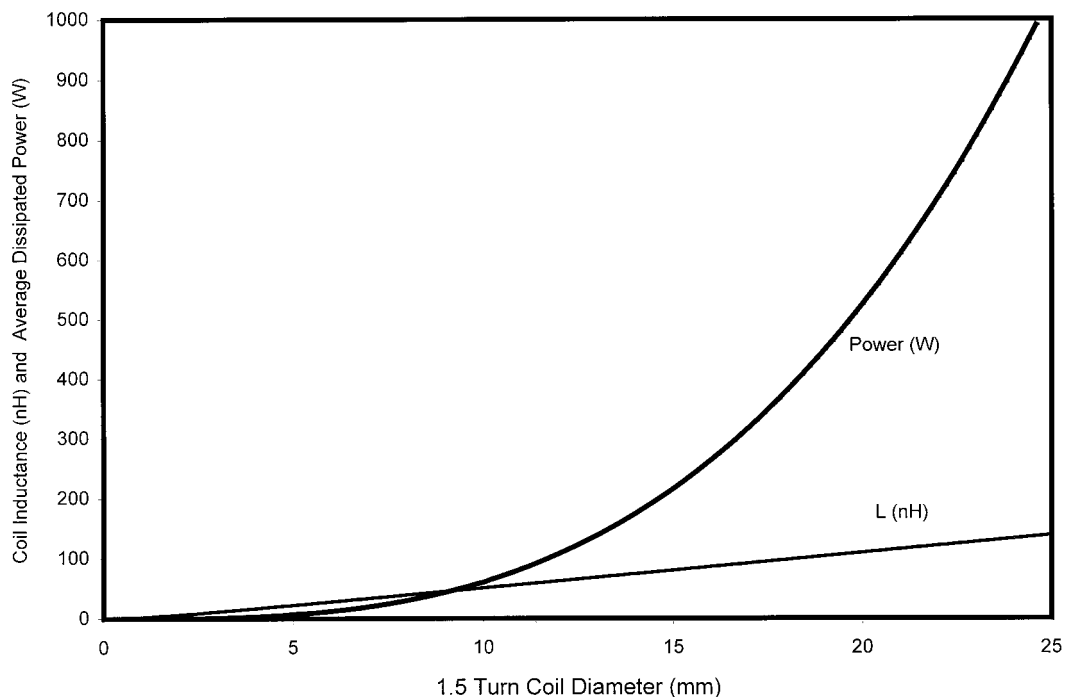
FIG. 5. Plot of the calculated average power dissipated in circuits similar to those shown in Figs. 2 and 4 as coil diameters are increased. The calculations assume circuit component values selected for 5-ns exponential time constants of 2.5-mT peak fields at 1% duty cycle for field coils from 5- to 25-mm diameter with one and a half turns each. Pairs of these coils in a Helmholtz configuration can deliver 5-mT fields with rise times on the order of 10 ns. The rapidly increasing power requirements as coil diameters are increased results from the larger currents and circuit resistances needed to maintain constant field and L/R ratio.

and f_0 is the resonance frequency. "Q switching" would, in principle, allow higher Q circuits to be employed while maintaining short dead time with the *caveat* that this can also be a source of transients.

Switching polarizing field transients aside, the absence of short high-power radio- or microwave frequency transmitter pulses reduces receiver saturation and the resulting spectrometer system dead time. In the experiment reported herein, high-frequency field switching components were minimized by shaping the switching current vs time profile to a relatively smooth 10-ns time constant exponential waveform to minimize Fourier components near the signal frequency of 185 MHz. The relatively high gate capacitance of the power MOSFET used here forms one element of a natural low-pass RF filter when combined with the gate driver circuit series resistance. The order of magnitude reduction of dead time compared to conventional pulsed EPR spectrometers presents many attractive features that will allow study of a wide selection of paramagnetic centers based on their physical, chemical, or biological merits rather than solely on favorable relaxation properties. This is especially true in experiments with spin labels where short relaxation times are often encountered.

In this spectrometer the clock signal driving the programmable pulse generator is derived from the frequency synthesizer clock so the receiver local oscillator maintains a constant phase with respect to the field switching pulses. Phase sensitive detection is therefore used to improve S/N and detect FID phase. Signal-to-noise improvements using digitized signal averaging at repetition periods on the order of T_1 are possible, but the field switching stability needs to be good enough to make full use of phase coherent detection. The present design does not have sufficient stability. Several possible solutions to this problem are being studied. Transforming the unstable time domain signals to the frequency domain and aligning the shifted spectral components prior to averaging in near real time may be possible with one of the newer fast digital signal processors. This requires a reference resonance signal that can be well quantified in a single acquisition.

Another improvement in dynamic magnetic field stability may be possible using an analog current feedback control circuit instead of the high-speed MOSFET switch and fixed series resistance circuit shown in Fig. 4b. Broadband operational amplifiers such as the Comlinear CLC220AI and CLC104AI have insufficient gain bandwidth, settling time, slew rates, and/or stability to drive a power MOSFET gate (capacitive load) with nanosecond rise time signals. However, improved devices are already available.

Roughly speaking, the component cost of the FFS spectrometer can be expected to scale with the sample volume and the magnetic field energy density ($\sim$volume $\times$ $\mathbf{B}_0^2$). Technology
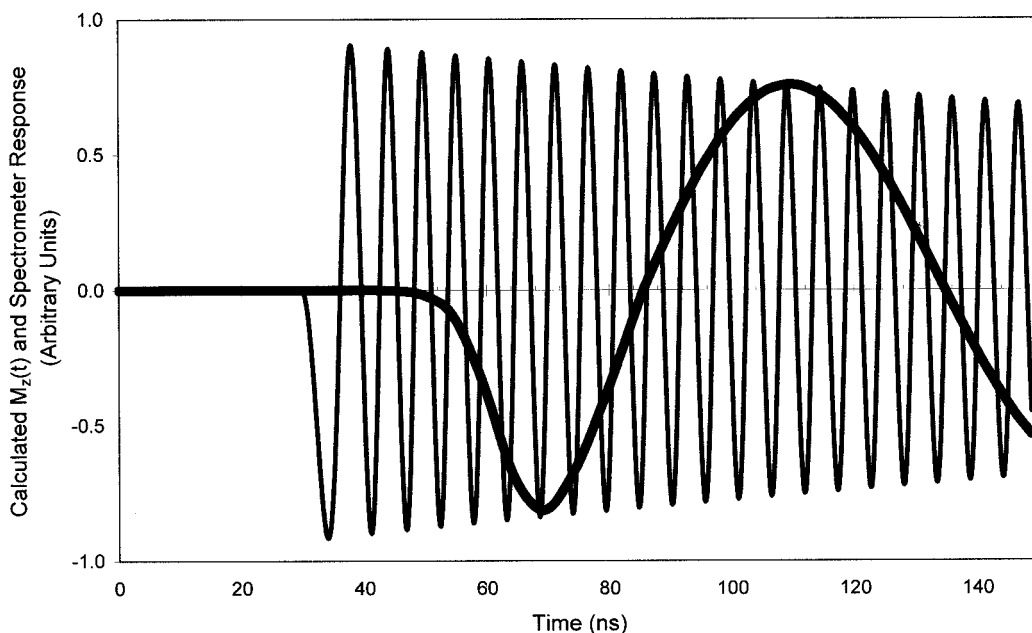
FIG. 6. Lighter shade trace is a depiction of a calculated solution to the modified Bloch equations discussed in Abragam (*2b*) for $M_z(t)$ during the time-dependent magnetic fields shown in Fig. 3. Depicted with a darker trace during same field switching interval are the calculated spectrometer outputs assuming a 195-MHz local oscillator reference frequency, 20-MHz bandwidth, RF pickup coil Q of 10 at 185-MHz resonance frequency, and no coupled field switching noise. Note that although $M_z(t)$ responds immediately to $B_x(t)$, the spectrometer response is delayed due to receiver bandwidth limitations. General features of the 150-ns time interval simulated signal are seen in the measured signal shown in Fig. 7.

continues to improve in high-speed, high-current switching transistors and expenses associated with fast field switching are expected to decrease. In addition to technological limitations, choice of appropriate polarization and/or precession field strengths will depend upon the application and system to be examined. Generally, maximal polarization magnetic fields are desirable for production of the greatest sample magnetization. Choice of the appropriate precession field strength will require consideration of the electrical characteristics of the sample (e.g., dielectric resonances and RF resistivity related signal losses can be issues with conducting samples at high frequencies) and the strength of any local interaction fields. A precession frequency of ca. 200 MHz was chosen herein because of this laboratory's interest in developing a larger scale FFS spectrometer for intact biological systems. Experience with nuclear magnetic resonance experiments on such systems suggests that conductive sample related problems are not prohibitive at this frequency. The FFS spectrometer in the present prototype form requires careful adjustment and will require modifications to scale up for larger samples. Figure 5 shows the calculated average power dissipation for similar circuits with field coils up to 25-mm diameter. As a final technical note, during the spectrometer setup, 0.5-mm^2 copper foil flux paddles were carefully positioned near opposite ends of the receiver coil to minimize the coupling of field switching transients from the field coils with the pickup coil.
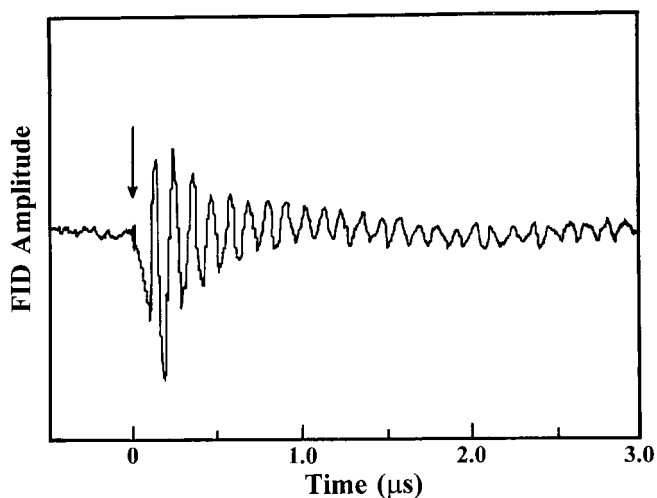

FIG. 7. A free induction decay of fluoranthenyl radical cation salt of PF_6 measured using the 185-MHz FFS spectrometer. The sample assembly is composed of several crystalas in a 1.5-mm-diameter pipette tip. The local oscillator frequency driving the receiver double-balanced mixer is 195 MHz. The signal "chirps" to the observed beat frequency between the spectrometer local oscillator and magnetic moment precession as the observation field exponentially approaches 6.6 mT. The signal is recorded in one "shot" of 2048 data digitization channels with 20 ns per channel by a Biomation waveform recorder. Experimental factors contributing to the observed nonexponential decay signal include the anisotropy of the multicrystalline sample and the inhomogeneity of the precessional (B_x) magnetic field.

CONCLUSION

A fast response field switching spectrometer has been described that places all spectral components of even broad EPR lines in the transverse plane for measurement as long as the nonadiabatic conditions are met. The receiver circuit used here is limited by bandwidth to spectral components less than about 10 MHz. The usual signal-to-noise compromise applies as the bandwidth is increased and induced switching noise will likely be a greater problem as well. If some of the benefits of digital signal averaging can be achieved as discussed above, the observation field could be scanned so the signal more effectively "chirps" through the spectral detection window. As noted earlier, preliminary work indicates that it may be necessary to include known reference spins along with the spin sample under study to obtain useful phase sensitive data using these techniques. Also noteworthy with this type of spectrometer is that signal intensity can be made greater by increasing the $\mathbf{B}_0$ polarizing field relative to a fixed $\mathbf{B}_0^*$ precessional field within the limits of the spectrometer components without affecting the low observation frequency benefits with regard to sample conductivity losses.

Other variations on this theme are envisaged as technology improves. This type of spectrometer may prove to be useful for measuring low-field spin relaxation processes, for example, by varying the time interval spent at low fields before nonadiabatically switching on the observation field. EPR imaging may prove feasible in the earth's field in a manner similar to that explored by Stepisnik *et al.* (*3*). Similar field switching circuits were used by this laboratory for fast field *sweeping* experiments that probed the spin dynamics at the level anticrossing region of the photo-excited triplet state of pentacene in *p*-terphenyl (*9*).

REFERENCES

1. M. E. Packard and R. Varian, Free nuclear induction in the earth's magnetic field, *Phys. Rev.* **93,** 941 (1954).

2. A. Abragam, The Principles of Nuclear Magnetism, *in* "The International Series of Monographs on Physics" (W. C. Marshall and D. H. Wilkinson, Eds.), pp (a) 65 and (b) 53, Oxford Univ. Press, London, (1961).

3. J. Stepisnik, V. Erzen, and M. Kos, NMR imaging in the earth's magnetic field, *Magn. Reson. Med.* **15,** 386 (1990).

4. B. F. Melton and V. L. Polak, Proton spin relaxation and exchange properties of hydrated chromic ions in H_2O and H_2O-D_2O mixtures, *J. Phys. Chem.* **73,** 3669 (1969).

5. A. G. Redfield, W. Fite, and H. E. Bleich, Precision high speed current regulators for occasionally switched inductive loads, *Rev. Sci. Instrum.* **39,** 710 (1968).

6. C. Job, J. Zajicek, and M. F. Brown, Fast field-cycling nuclear magnetic resonance spectrometer, *Rev. Sci. Instrum.* **67,** 2113 (1996).

7. E. Rommel, K. Mischker, G. Osswald, K. H. Schwikert, and F. Noack, A powerful NMR field-cycling device using GTOs and MOSFETs for relaxation dispersion and zero-field studies, *J. Magn. Reson.* **70,** 219 (1986).

8. B. F. Melton, V. L. Pollak, T. W. Mayes, and B. L. Willis, Condition for sudden passage in the earth's field NMR technique, *J. Magn. Reson. A* **117,** 164 (1995).

9. V. Kouskov, D. J. Sloop, S. I. Weissman, and T.-S. Lin, Adiabatic passage through an avoided crossing, *Chem. Phys. Lett.* **232,** 165 (1995).